PNAS RESEARCH ARTICLE | BIOCHEMISTRY

Structural insights into constitutive activity of 5-HT$_6$ receptor

Licong He[a,1], Qiaoyu Zhao[a,1], Jianzhong Qi[a,1], Yifan Wang[a,1], Wenyu Han[a], Zhangcheng Chen[a], Yao Cong[a,2], and Sheng Wang[a,2]

Edited by Zhi-Jie Liu, ShanghaiTech University, Shanghai, China; received June 9, 2022; accepted February 16, 2023 by Editorial Board Member Nieng Yan

While most therapeutic research on G-protein-coupled receptors (GPCRs) focuses on receptor activation by (endogenous) agonists, significant therapeutic potential exists through agonist-independent intrinsic constitutive activity that can occur in various physiological and pathophysiological settings. For example, inhibiting the constitutive activity of 5-HT$_6$R—a receptor that is found almost exclusively in the brain and mediates excitatory neurotransmission—has demonstrated a therapeutic effect on cognitive/memory impairment associated with several neuropsychiatric disorders. However, the structural basis of such constitutive activity remains unclear. Here, we present a cryo-EM structure of serotonin-bound human 5-HT$_6$R-Gs heterotrimer at 3.0-Å resolution. Detailed analyses of the structure complemented by comprehensive interrogation of signaling illuminate key structural determinants essential for constitutive 5-HT$_6$R activity. Additional structure-guided mutagenesis leads to a nanobody mimic Gαs for 5-HT$_6$R that can reduce its constitutive activity. Given the importance of 5-HT$_6$R for a large number of neuropsychiatric disorders, insights derived from these studies will accelerate the design of more effective medications, and shed light on the molecular basis of constitutive activity.

GPCR | serotonin receptor | cryo-EM | constitutive activity | 5-HT$_6$R

Significance

GPCR display agonist-independent signaling transduction that is known as constitutive activity. 5-HT$_6$R has a high level of constitutive activity which is related to the therapy of neuropsychiatric disorders. However, the mechanism of constitutive activity is still poorly understood. Therefore, we report serotonin-bound 5-HT$_6$R-Gs complex structure, and illuminate the two structural determinants required for constitutive 5-HT$_6$R activity: 1) The interhelical hydrogen bond between T280$^{6.47}$ and N312$^{7.45}$ in 5-HT$_6$R that abolished the negative allosteric modulator-Na$^+$ and 2) a pair of equally charged amino acids (R325$^{8.48}$ from the receptor/R389 from Gαs) that experienced a repulsive force to facilitate receptor activation. This structural information has enabled the design of a receptor-specific nanobody-NB6A1 that was found to reduce the receptor's basal activity.

Serotonin receptors are activated by the important neurotransmitter serotonin (or 5-hydroxytryptamine, 5-HT), which are involved in the regulation of virtually all brain functions. Dysregulation of the serotonergic system has been implicated in the pathogenesis of many psychiatric and neurological disorders (1–3). Except for the 5-HT$_3$ receptor, which is a ligand-gated ion channel, 5-HT receptors belong to the G-protein-coupled receptor (GPCR) superfamily and, with at least 13 distinct members, represent one of the most complex families of neurotransmitter receptors. 5-HT receptors have been divided into seven major classes (5-HT$_{1\text{-}7}$R) based on their structural, functional, and pharmacological characteristics (1, 2). The 5-HT$_6$R is among the latest identified members of the 5-HT receptor family (4, 5) and is a particularly interesting receptor subtype because of its relatively low level of sequence homology (<50%) compared to other serotonin receptors and exclusive distribution in the central nervous system (6). Although the mechanisms associated with the 5-HT$_6$R activation/blockade are not completely understood, its ligands have demonstrated therapeutic effect on neuropsychiatric disorders, including Alzheimer's disease and schizophrenia (7–10).

It is well known that 5-HT$_6$R displays a high level of ligand-independent constitutive activity (11, 12), and this activity has been related to neuronal development, neocortical radial migration, and self-renewal of human neural stem cell (13–16). According to the two-state model of receptor activation, receptors in a population were thought to exist in equilibrium with an inactive (R) and active conformation (R*) (17). While it is now generally accepted that most, if not all, receptors possess some level of constitutive receptor activity, the precise mechanism of constitutive activity remains largely unknown. In addition, no structure of 5-HT$_6$R has been reported, limiting a mechanistic understanding of agonist binding and receptor activation, and thus hindering structure-based drug discovery targeting the 5-HT$_6$R. In the present study, we report the cryo-EM structure of serotonin-activated 5-HT$_6$R in complex with heterotrimeric protein, Gs-coupled, to unveil the mechanism of agonist binding and ligand-induced receptor activation. Through a comparative analysis of 5-HT$_6$R and other Gs-coupled GPCRs structures, this study provides comprehensive insights into the constitutive activity of 5-HT$_6$R.

Results

Overall Cryo-EM Structure of Serotonin-Bound 5-HT$_6$R-Gs Complex. To obtain the serotonin-bound 5-HT$_6$R in complex with Gs, we purified serotonin-bound 5-HT$_6$R and mixed it with Gs heterotrimer. Due to 5-HT$_6$R's longer and more flexible intracellular loop 3 (ICL3), the expression yield of the complex was quite low and unstable. In this study, we tried different truncations of ICL3 and added soluble fusion proteins at the

Author contributions: Y.C. and S.W. designed research; L.H., Q.Z., J.Q., Y.W., W.H., and Z.C. performed research; L.H., Q.Z., J.Q., Y.W., Y.C., and S.W. analyzed data; and S.W. wrote the paper.

The authors declare no competing interest.

This article is a PNAS Direct Submission. Z.-J.L. is a guest editor invited by the Editorial Board.

[1]L.H., Q.Z., J.Q., and Y.W. contributed equally to this work.

[2]To whom correspondence may be addressed. Email: cong@sibcb.ac.cn or wangsheng@sibcb.ac.cn.

This article contains supporting information online at https://www.pnas.org/lookup/suppl/doi:10.1073/pnas.2209917120/-/DCSupplemental.

Published March 29, 2023.

N terminus. Eventually, we were able to improve the expression level of 5-HT_6R by inserting BRIL protein at the N terminus, and the stable complex was successfully assembled by removing residues S231-E248 of ICL3 and parts of the C-terminal (*SI Appendix,* Fig. S1*A*). In addition, 25 amino acids at the N terminus of Gαs were replaced by the corresponding sequence in $G\alpha i_1$ to facilitate binding of a single-chain variable fragment (scFv16) (18), thereby further stabilizing the 5-HT_6R-Gs protein complex for structural studies (*SI Appendix,* Fig. S1 *B* and *C*). An analogous approach was recently used to obtain structures of the M_1–muscarinic receptor–G_{11} complex and the 5-HT_{2A}R-Gq complex (19, 20).

The full complex of 5-HT_6R-$G\alpha s_{iN}$/$G\beta_1$/$G\gamma_2$ was then assembled in the presence of the serotonin and further stabilized by the single-chain antibody scFv16 and the addition of camelid antibody, Nb35, which binds at the Gαs–Gβ interface and was used in the determination of the β_2 adrenergic receptor (β_2AR)–Gs heterotrimer structure (21) (*SI Appendix,* Fig. S1*B*). The structure of 5-HT_6R complexed with serotonin was determined by cryo-EM single-particle analysis at a global nominal resolution of 3.0 Å, enabling near-atomic resolution modeling of the complex (Fig. 1 *A* and *B* and *SI Appendix,* Figs. S2–S4 and Table S1). The density map is sufficiently clear to place 5-HT_6R, the three G protein subunits, scFv16, and serotonin in it (Fig. 1 *A* and *B* and *SI Appendix,* Figs. S2 and S4). Although we included Nb35 in the 5-HT_6R-$G\alpha s_{iN}$/$G\beta_1$/$G\gamma_2$ sample for cryo-EM study, no obvious density corresponding to this nanobody was observed at the Gαs–Gβ interface or other

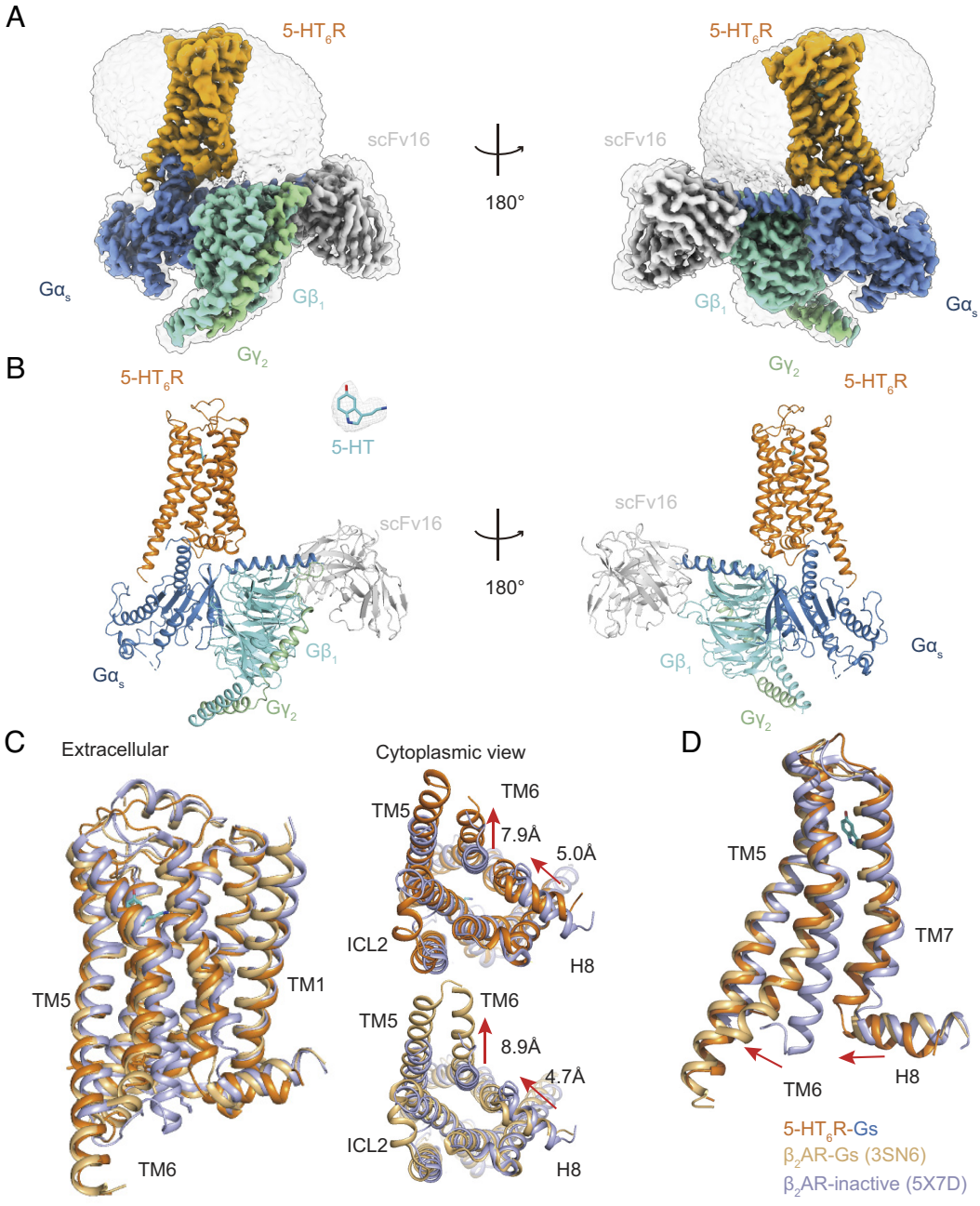

Fig. 1. Cryo-EM structure of the serotonin-bound 5-HT_6R-Gs complex. (*A*) Cryo-EM map of the serotonin-bound 5-HT_6R-Gs complex. Colored by subunits (5-HT_6R in orange, Gαs in cornflower blue, Gβ in aquamarine, Gγ in light green, scFv16 in light gray, and serotonin in cyan). (*B*) Cartoon diagram of the serotonin-bound 5-HT_6R-Gs complex. Ligand is shown at the *Upper Right* side of the complex in the *Left* panel, with corresponding density also shown. Color schemes are the same as in *A*. (*C*) Side (*Left*), and cytoplasmic (*Right*) views of the active 5-HT_6R (orange) and active β_2AR (PDB: 3SN6, light orange) relative to inactive β_2AR (PDB: 5X7D, blue) structures. Differences in transmembrane domains are highlighted. (*D*) Zoomed-in views of TM6, TM7 and H8 are shown for Gs-stabilized 5-HT_6R (orange) and Gs-stabilized β_2AR (PDB: 3SN6, light orange).

regions (Fig. 1*A* and *SI Appendix*, Fig. S2). The overall structure of serotonin-stabilized 5-HT$_6$R-Gαs_{iN}/β_1/γ_2 structure is consistent with the fully active-state receptor conformation that has been observed in several other GPCRs bound to a G-protein ternary complex (22). We found that scFv16 binds to the crevice between the αN helix of Gαs_{iN} and the β-propeller of Gβ_1 similar to that observed in the MOR-Gi complex (23), thereby providing additional stabilization of the complex (Fig. 1 *A* and *B*).

Potential Mechanisms of 5-HT$_6$R Activation. The overall structure of the active 5-HT$_6$R is similar to that of the active conformation of β_2AR (Fig. 1*C*), with RMSD values (calculated by Cα atoms) of 0.75 Å for the whole complex, 1.04 Å when comparing with receptors alone, and 0.74 Å when comparing with G proteins alone. Since β_2AR is aminergic receptor and recruits Gs protein like 5-HT$_6$R, which has inactive and active state structure, we have subsequently compared the structure of the 5-HT$_6$R with that of β_2AR. When comparing inactive β_2AR (24) and active states of 5-HT$_6$R, the largest structural changes upon Gs engagement occur in the cytoplasmic side of 5-HT$_6$R, with an outward rotation of TM6 by 7.9 Å (measured between the Cα of K265$^{6.32}$ of 5-HT$_6$R and the Cα of K270$^{6.32}$ of inactive β_2AR) and an inward 5.0 Å movement of TM7 (measured between the Cα of Y320$^{7.53}$ of 5-HT$_6$R and the Cα of Y326$^{7.53}$of inactive β_2AR) (Fig. 1 *C* and *D*). The TM6 movement is accompanied by a small rotation of the helix, as well as a tilt of TM5 toward TM6. These structural changes allow the C-terminal helix of the α subunit of the G protein to engage the receptor core (Fig. 1*B*). Although most class A GPCRs adopted the similar inactive structure conformation, the exact conformation difference between active and inactive 5-HT$_6$R still needs inactive 5-HT$_6$R structure to validate. Additionally, ICL2 forms a short α helix, which is a common feature of the Class A GPCRs within G-protein complexes (Fig. 1*C*).

The conformations of critical residues for receptor activation, such as D$^{3.49}$R$^{3.50}$Y$^{3.51}$, N$^{7.49}$P$^{7.50}$xxY$^{7.53}$, C$^{6.47}$W$^{6.48}$xP$^{6.50}$, and P$^{5.50}$I$^{3.40}$F$^{6.44}$ motifs (superscripts indicate Ballesteros-Weinstein numbering), are also similar between active conformations of 5-HT$_6$R and β_2AR (*SI Appendix*, Fig. S5), suggesting that the activation mechanism is shared between the serotonin and adrenergic receptors. To clarify the molecular mechanisms of 5-HT$_6$R activation, we investigated in detail how conformational changes are likely propagated between serotonin and transducer binding sites (Fig. 2). In the serotonin-bound 5-HT$_6$R structure, serotonin not only forms a salt bridge with D106$^{3.32}$, which is a critical interaction for ligand binding in serotonin and other monoamine receptors (25), but it also triggers a downward force on the indole ring of W281$^{6.48}$ (Figs. 2*B* and 3*A*). In the 5-HT$_6$R active state, residue W281$^{6.48}$, a highly conserved toggle switch, forms both the hydrophobic contacts with F277$^{6.44}$ in the P$^{5.50}$I$^{3.40}$F$^{6.44}$ motif (Fig. 2*C*), a central "microswitch" for the activation of many GPCRs (26), and the hydrogen bond with N312$^{7.45}$ in the negative allosteric modulator Na$^+$ pocket (D$^{2.50}$, C$^{3.35}$, S$^{3.39}$, N$^{7.45}$ and N$^{7.49}$, Fig. 2 *C* and *D*) (27). Facilitated by the downward swing of W281$^{6.48}$ in the active state, F277$^{6.44}$ rotates its benzyl ring outward and N312$^{7.45}$ shifts toward the Na$^+$ pocket. This action collapses the Na$^+$ pocket upon activation, causing N312$^{7.45}$ to form instead a hydrogen bond with N316$^{7.49}$ (Fig. 2 *C* and *D*). Through this hydrogen bond, the sodium pocket is further directly coupled to the N$^{7.49}$P$^{7.50}$xxY$^{7.53}$ motif at the intracellular tip of TM7, which cascades downward to the conformational changes of N316$^{7.49}$ and Y320$^{7.53}$, leading to a large outward swing of TM6's cytoplasmic end and mild inward shift of TM7's cytoplasmic end (27, 28) (Fig. 2*E*).

As a consequence of the above conformational relays, and in association with the Gs binding, the salt bridge between D123$^{3.49}$ and R124$^{3.50}$ in the D$^{3.49}$R$^{3.50}$Y$^{3.51}$ motif, which is characteristic for many inactive state structures, is broken in the 5-HT$_6$R active state, and instead R124$^{3.50}$ points toward the receptor core (Fig. 2 *A* and *F*). A similar configuration of R$^{3.50}$ has previously been observed in the structures of β_2AR bound to a heterotrimeric G protein (21) (*SI Appendix*, Fig. S6*A*), adenosine A$_2$A receptor bound to a thermostabilized "mini-Gs" (29) (*SI Appendix*,

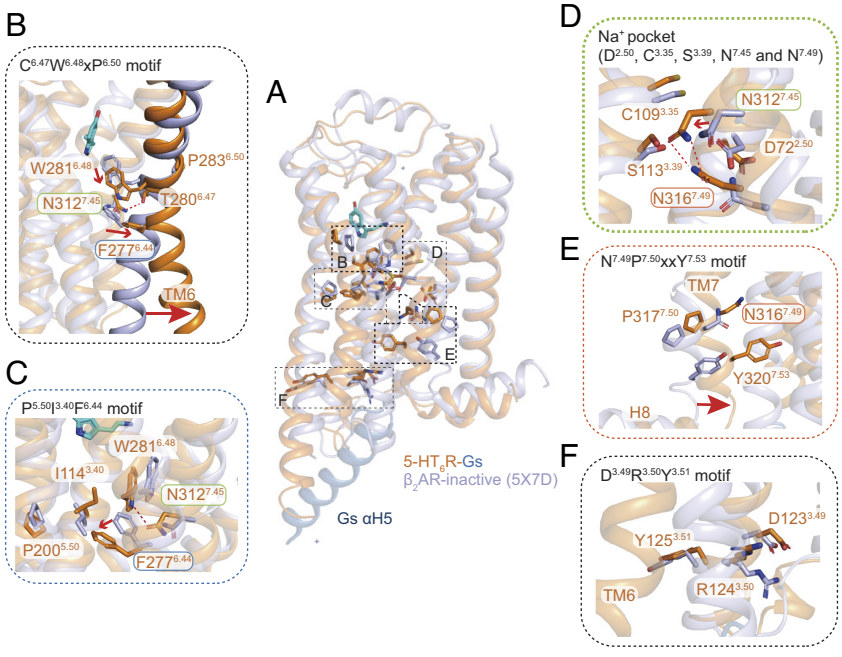

Fig. 2. Activation motifs of 5-HT$_6$R. (*A*) Close-ups highlight activation-related conformational changes in key receptor motifs and show the connection of structural changes from the orthosteric site to the cytoplasmic transducer binding site. Conformational changes between active 5-HT$_6$R (orange) and inactive β_2AR (blue) are highlighted for (*B*) CWxP motif, (*C*) P-I-F motif, (*D*) sodium binding pocket, (*E*) NPxxY motif, and (*F*) DRY motif. The side chain of residues in motifs are shown as sticks. Hydrogen bond are shown with red dotted line. Red arrows indicate the shift directions in active 5-HT$_6$R relative to inactive β_2AR.

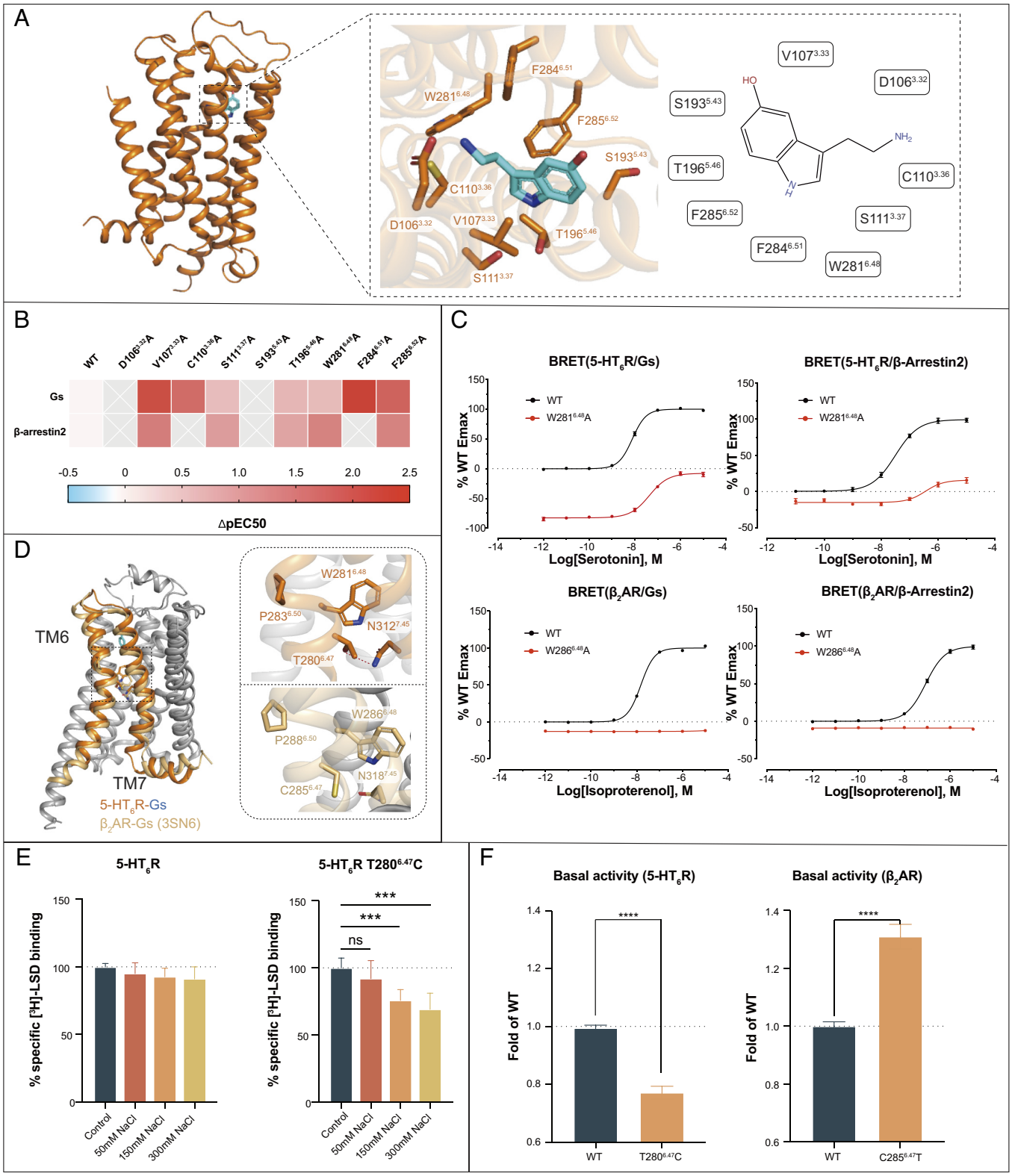

Fig. 3. Molecular recognition of serotonin by 5-HT$_6$R. (*A*) Conformation of the binding pocket of 5-HT$_6$R, with serotonin shown as sticks with cyan carbons. The protein is displayed in cartoon representation, with the nine contact residues within 4.0 Å from the ligand shown as orange sticks. (*B*) Mutagenesis studies showing the effects of orthosteric-site residues on functional activity. Heatmap of ΔpEC_{50} (EC_{50WT}-EC_{50mt}) (by BRET, 5-HT$_6$R/mini-Gs, and 5-HT$_6$R/β-arrestin2). See *SI Appendix*, Fig. S3 *A* and *C* for fitted parameter values that represent mean ± SEM of n = 3 biological replicates. (*C*) Effects of W$^{6.48}$A mutant in 5-HT$_6$R and β_2AR on recruitment of mini-Gs and β-arrestin2. Data are mean ± SEM of n = 3 biological replicates. (*D*) Comparison of the C/TWxP motif in the 5-HT$_6$R (orange) and active β_2AR (light orange). T280$^{6.47}$ forms hydrogen bond with N312$^{7.45}$ in 5-HT$_6$R. (*E*) [^{3}H]-LSD equilibrium binding to 5-HT$_6$R and 5-HT$_6$R-T$^{6.47}$C mutant in the presence of buffer (control) or buffer supplemented with NaCl. (*F*) The basal activity of T280$^{6.47}$C (5-HT$_6$R) and C285$^{6.47}$T (β_2AR) is compared to its wild type (WT), respectively. The figures represent data combined from three separate experiments performed in duplicate (*E* and *F*). Significant differences were observed for the effect of modulators on control binding (Student's *t* test, ns: not significant, ***$P < 0.001$, ****$P < 0.0001$).

Fig. S6*B*) and M_2 muscarinic receptor bound to β-arrestin1 (30) (*SI Appendix,* Fig. S6*C*), but a different configuration in the β_1AR bound to β-arrestin1 (31) (*SI Appendix,* Fig. S6*D*). Overall, 5-HT_6R undergoes a similar activation process mediated through the signature motifs conserved in class A GPCRs.

Structural Motif Associated with the Constitutive Activity of 5-HT_6R. Serotonin binds to the activated 5-HT_6R in a similar orientation to that observed in recently solved serotonin-bound 5-HT_{1A}R and 5-HT_{1D}R structures (32) (Fig. 3*A* and *SI Appendix,* Fig. S7 *A–D*). Unsurprisingly, the mutation of $D106^{3.32}$ leads to a loss of serotonin function and binding (Fig. 3*B* and *SI Appendix,* Table S2). Other interactions have also been observed in the structure, such as $V107^{3.33}$, $C110^{3.36}$, $S111^{3.37}$, $S193^{5.43}$, $T196^{5.46}$, $W281^{6.48}$, $F284^{6.51}$, and $F285^{6.52}$ (Fig. 3*A* and *SI Appendix,* Fig. S7 *E* and *F*). Our mutagenesis and functional experiments suggested that many of these residues are essential for ligand binding and subsequent receptor activation as measured using bioluminescence resonance energy transfer (BRET) analyses to determine by mini-Gs or β-arrestin2 association and cAMP accumulation assay (Fig. 3*B* and *SI Appendix,* Fig. S8*A* and Table S2). In all mutants, the expression level of 5-HT_6R is comparable to that of wild-type, except $F285^{6.52}$A mutation which reduces the expression level. (*SI Appendix*, Fig. S8*B*).

The residues that coordinate osteric binding site and the $C^{6.47}W^{6.48}xP^{6.50}$ motif "toggle switch" are implicated in GPCR activation. Therefore, given this intimate relationship, it is not surprising that the previous mutagenesis data showed that mutation of the $W^{6.48}$ toggle switch abolished the ligand's activity for many class A GPCRs, such as 5-HT_{1A}R, 5-HT_{2A}R, DRD1, and DRD2 (20, 32–34). Indeed, our data also showed that mutating $W^{6.48}$ into alanine abolished the ligand's G-protein signaling and β-arrestin2 recruitment activity at β_2AR (Fig. 3*C*). However, the $W281^{6.48}$A mutant of 5-HT_6R reserved the efficacy of serotonin's Gs agonism and abolished serotonin's β-arrestin2 recruitment activity (Fig. 3*C* and *SI Appendix,* Table S2). Further analysis of the $W281^{6.48}$A mutant also maintained serotonin's efficacy in Gs function as assessed by cAMP accumulation assay (*SI Appendix,* Fig. S8*C*). By contrast, the $W281^{6.48}$A substitution also abolished serotonin's β-arrestin2 recruitment activity, employing an orthologous platform for arrestin recruitment using the Tango system (*SI Appendix,* Fig. S8*C*).

Unlike most class A GPCRs, which are fully conserved at the $C^{6.47}W^{6.48}xP^{6.50}$ motif, 5-HT_6R has a polar residue threonine (T) at 6.47. The position of 5-HT_6R's TM6 appears fixed by a hydrogen bond between $T^{6.47}$ and $N^{7.45}$, whereas in most class A GPCRs, such as β_2AR, $C^{6.47}$ cannot form a hydrogen bond with $N^{7.45}$ (Fig. 3*D*). Given the critical nature of TMs 6 and 7 in GPCR activation, we wondered whether this added hydrogen bond restraint has functional consequences. The $T280^{6.47}$C mutation in 5-HT_6R, mimicking the conserved $C^{6.47}W^{6.48}xP^{6.50}$ motif, still maintained ligand-dependent Gs function and β-arrestin2 recruitment activity (*SI Appendix,* Fig. S8*D*). Also, the $C285^{6.47}$T mutation in β_2AR, recapitulating 5-HT_6R's interhelical hydrogen bond, maintained ligand-dependent Gs function and β-arrestin2 recruitment activity (*SI Appendix,* Fig. S8*D*).

Previous studies have shown that the second coordination shell of the sodium ion in the allosteric site is formed by the side chains of three residues ($W^{6.48}$, $N^{7.45}$, and $N^{7.49}$) (35). These conserved residues of the sodium pocket belong to two of the most well-known class A functional motifs: $C^{6.47}W^{6.48}xP^{6.50}$ in TM6 and $N^{7.49}P^{7.50}xxY^{7.53}$ in TM7 (Fig. 2 *B–E*). To clarify the nature of sodium's negative cooperativity to the agonist, we performed [^{3}H]-lysergic acid diethylamide ([^{3}H]-LSD) binding assays with and without sodium at 5-HT_6R. We found that sodium produced negative cooperativity with the agonist [^{3}H]-LSD at the $T280^{6.47}$C mutant, but not the wild-type 5-HT_6R (Fig. 3*E*). Most of the published results are consistent with the notion that sodium stabilizes the inactive state and thereby reduces basal G protein activity (27, 36). Also, the constitutive activity of GPCRs can be dramatically affected by mutations in sodium-coordinating residues (27). Indeed, we found that the $T280^{6.47}$C mutant recaptured sodium's negative cooperativity, significantly reducing the basal activity of 5-HT_6R (Fig. 3*F* and *SI Appendix,* Fig. S8 *B* and *E*). BRET ratio without drug addition was used to represent the basal activity, which wasn't affected by the expression level of the receptor (*SI Appendix,* Fig. S9 *A* and *B*). In contrast, the $C285^{6.47}$T mutant increased β_2AR constitutive activity (Fig. 3*F* and *SI Appendix,* Fig. S8 *B* and *E*). And, compared with β_2AR and DRD1 (without the hydrogen bond between $C^{6.47}$ and $N^{7.45}$), 5-HT_6R displayed a high level of basal activity at both BRET and cAMP accumulation assay (*SI Appendix,* Fig. S10 *A–C*).

The hydrogen bond between $T280^{6.47}$ and $N312^{7.45}$ not only disrupted the sodium pocket, but also impaired the movement of $N312^{7.45}$. And in the activated 5-HT_6R structure, $N312^{7.45}$ formed the hydrogen bond with $W281^{6.48}$, as well with $N316^{7.49}$ in Na^+ pocket and NPxxY motif (Fig. 2 *C* and *D*). It is not surprising that $N312^{7.45}$L mutant abolished both serotonin's Gs agonism and β-arrestin2 recruitment activity (*SI Appendix,* Fig. S8*F*). Overall, the activated agonist-bound structure of 5-HT_6R reveals a sodium site that is collapsed by a downward swing of $W^{6.48}$ and inward movement of $N^{7.45}$ and $N^{7.49}$, suggesting that rearrangements in this conserved sodium pocket have a key role in the activation of class A GPCRs. By contrast, the collapsed sodium pocket of 5-HT_6R appears fixed by a hydrogen bond between $T^{6.47}$ and $N^{7.45}$, which partially explains 5-HT_6R's high levels of constitutive activity.

Contributions of TM7 and Helix 8 to 5-HT_6R Activation. Globally, the structure of the 5-HT_6R-Gs complex reveals a similar mode of interaction when compared to other Gs-bound receptors, such as β_2AR and Dopamine D_1 receptor (DRD1) (Fig. 4 *A* and *B* and *SI Appendix,* Fig. S11*A*). However, when aligned on the receptors, the 5-HT_6R structure displays a larger inward movement of TM7 and H8 relative to the β_2AR-Gs and DRD1-Gs complexes (Figs. 1*D* and 4*C* and *SI Appendix,* Fig. S11*B*), with the α5-helix of the Gαs closer to TM7 and helix 8 of the receptor.

Previous studies have suggested that GPCRs interact and activate Gα subunits through a highly conserved mechanism in which the interruption of the contacts between H1 and H5 is a key step for GDP release (37, 38). While H1 is the molecular switch for GDP release, H5 is the distal trigger that is "pulled" upon receptor binding (*SI Appendix,* Fig. S11*C*). H1 acts as a structural "hub" by linking different functional regions of Gα in the inactive state, forming contacts both to GDP, via the Walker A motif, and to H5, through the π–π stack (37). In the 5-HT_6R-Gs complex structure, consistent with other class A GPCR (37), the C-terminal of H5 undergoes a disorder-to-order transition in the intracellular cavity of the receptor (Fig. 4*D*). And, the H1 of Gαs for the 5-HT_6R-Gs complex undertakes the order-to-disorder transition, ultimately facilitating GDP release (Fig. 4*D* and *SI Appendix,* Fig S11*C*).

In the 5-HT_6R structure, due to the larger inward movement of TM7 and H8, $R325^{8.48}$ shifted closer to R389 (G.H5.21) of the Gαs protein (Fig. 4*E* and *SI Appendix,* Fig. S11*D*). Since the G-protein engagement is a complex process that involves several states, the repulsive force between the $R325^{8.48}$ and R389 (G.H5.21 Gαs) may facilitate the state transition and contribute the receptor activation. Indeed, compared to the wild-type

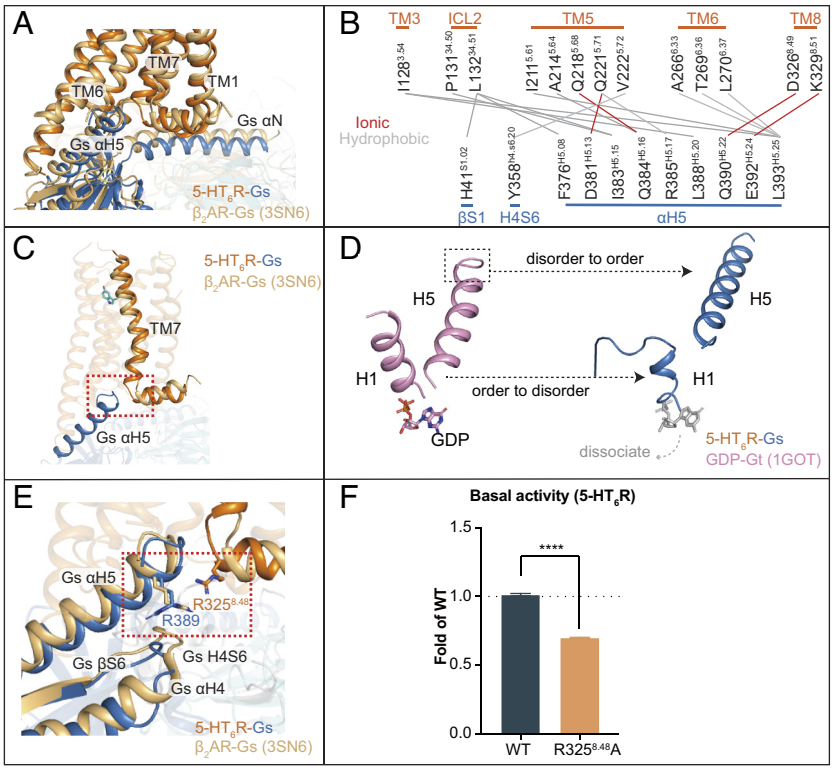

Fig. 4. The binding interface between 5-HT$_6$R and Gαs. (*A*) Superposition of 5-HT$_6$R (orange)-Gs (blue) and β_2AR-Gs (light orange) based on an alignment of the receptor. (*B*) Diagram of contacts between Gαs and 5-HT$_6$R. Ionic interactions are illustrated by red lines and hydrophobic interactions are illustrated by gray lines. (*C*) The larger inward movement of TM7 and H8 in 5-HT$_6$R (orange) than in active β_2AR (light orange). (*D*) The H1 and H5 of inactive Gt (1GOT, pink) and active Gαs in 5-HT$_6$R (blue). (*E*) α5-helix of the Ras-like domain of Gαs docks into a 5-HT$_6$R intracellular face cavity by the inward movement of R325$^{8.48}$. (*F*) The basal activity of R325$^{8.48}$A (5-HT$_6$R) is compared to its wild type (WT). Data are mean ± SEM of n = 3 biological replicates. Significant differences were observed for the effect of modulators on control binding (Student's *t* test, ****P < 0.0001).

5-HT$_6$R, the R325$^{8.48}$A mutant substantially reduced the basal G-protein activity of 5-HT$_6$R (Fig. 4*F*). However, the R389A (G.H5.21) of Gαs mutant abolished the G protein singaling at both 5-HT$_6$R and β_2AR, despite similar expression levels relative to the wild-type Gαs (*SI Appendix*, Fig. S11 *E* and *F*). Substitution of R389 with alanine may impair general activation of Gαs and R389 may also involve in the early interaction between receptor and G protein (39). And, In summary, the larger inward movements of TM7 and H8 were significantly correlated with 5-HT$_6$R's high levels of constitutive activity.

Structure-Based Rational Design of 5-HT$_6$R's Nanobody. When comparing β_2AR in complex with NB6B9 to β_2AR in complex with Gs, the CDR3 loop of nanobody NB6B9, which inserts into the receptor, bears a strong resemblance to the loop at the C terminal of the α5 helix of Gαs (Fig. 5*A*). Since Y107 of NB6B9 is located in the similar position with Gαs' R389(G.H5.21) (Fig. 5*B*), we wondered whether Y107R/H/K/E/D NB6B9 mutants could engage the active 5-HT$_6$R. We hypothesized that the mutations of Y107 to positively charged amino acids (R/H/K) in NB6B9 might experience a repulsive force with the R325$^{8.48}$ of 5-HT$_6$R, which could further induce the outward rotation of TM6 (*SI Appendix*, Fig. S12*A*). We found that, indeed, the Y107K NB6B9 mutant (NB6A1) was recruited in an agonist-dependent manner to 5-HT$_6$R, but not the wild-type NB6B9 and Y107R/H NB6B9 mutants (Fig. 5*C* and *SI Appendix*, Fig. S12*B*). Not surprisingly, the mutations of Y107 to negatively charged amino acids (E/D) in NB6B9 didn't work as expect (*SI Appendix*, Fig. S12*B*). To confirm the critical role of 5-HT$_6$R's R325$^{8.48}$ in NB6A1 binding, we performed a similar nanobody recruitment assay at the R325$^{8.48}$A mutant of 5-HT$_6$R. As expected, NB6A1's activity was decreased with the R325$^{8.48}$A mutant of 5-HT$_6$R (*SI Appendix*, Fig. S12*C*). Since a nanobody occupied 5-HT$_6$R's G protein binding site, NB6A1 sterically inhibited Gs binding and reduced the receptor's basal activity (Fig. 5*D* and *SI Appendix*, Fig. S12*D*). These results confirmed our hypothesis that conformationally selective nanobody could be identified through an integrative approach combining structure-based and mechanism-driven screening.

Discussion

Here, we have presented the cryo-EM structure of the 5-HT$_6$R-Gs complex bound to endogenous ligand serotonin and have provided detailed molecular insights into 5-HT$_6$R activation and basal activity. Using a combination of structural analysis, binding, and functional studies, we identified important 5-HT$_6$R receptor residues involved in the ligand-independent constitutive activity of 5-HT$_6$R. For instance, we showed that replacing T$^{6.47}$ in the toggle switch motif of 5-HT$_6$R with C$^{6.47}$ found in other class A GPCRs (CWxP motif), significantly reduced the basal activity of the 5-HT$_6$R and vice versa. Additionally, we found that the interhelical hydrogen bond between T$^{6.47}$ and N$^{7.45}$ may partially confer the high basal activity of the 5-HT$_6$R, consistent with observations that T$^{6.47}$C mutant, not the wild-type, displayed sodium-dependent allosteric regulation.

The interaction analysis of the 5-HT$_6$R-Gs complex revealed a core hydrophobic interface formed by the packing of the Gα α5 helix against a hydrophobic patch with the cytoplasmic ends of TM5 and 6, a feature reported previously for the most active state structure of GPCRs. A notable feature is the distinct location of the cytoplasmic ends of TM7 relative to that in β_2AR and DRD1. This is particularly interesting as R325$^{8.48}$, adjacent to TM7, shifts closer to R389 (G.H5.21) of the Gαs protein. Surrounding this repulsive force is the charge-incompatible 5-HT$_6$R and Gαs

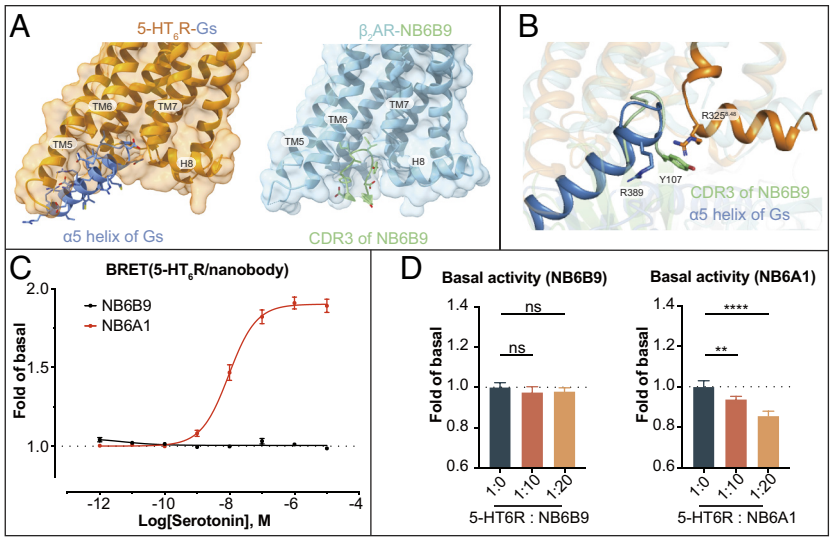

Fig. 5. Structure-guided discovery of 5-HT$_6$R's nanobody. (*A*) Comparison of the structures of 5-HT$_6$R-Gs and β_2AR-NB6B9 to highlight the similar position between the α5 helix of Gs and the CDR3 of NB6B9. (*B*) Details of coupled NB6B9 CDR3 loop and Gαs protein α5 helix after alignment of the receptors. (*C*) The difference of recruitment by 5-HT$_6$R between NB6B9 and NB6A1. Data are mean ± SEM of n = 3 biological replicates. (*D*) The basal activity of 5-HT$_6$R was reduced by the NB6A1, not the NB6B9. Significant differences were observed for the effect of modulators on control binding (Student's *t* test, ns: not significant, $^{**}P < 0.01$, $^{****}P < 0.0001$).

surface areas, with its leading to significantly enhanced constitutive activity of 5-HT$_6$R. Mimicking this repulsive force, the modification of the CDR3 of NB6B9, represents a viable path toward generating a receptor-specific nanobody. Molecular insights into these mechanisms may fully explain the high basal activity of the 5-HT$_6$R. Additionallly, this approach potentially provides a straightforward path for investigating the constitutive activity of other class A GPCRs.

Materials and Methods

Protein Expression and Purification. The human 5-HT$_6$R fused to an N-terminal BRIL protein with a truncated N terminus, ICL3 and C terminus, the dominant-negative Gαs (DNGαs) with a replaced N terminus by Gαi and the scFv16 were expressed and purified from sf9 insect cells. And the NB35 with His-tag at the C terminus was expressed in *Escherichia coli* BL21 cells and purified as described previously (40). After purification, the components in complex consisting of 5-HT$_6$R, DNGs, Nb35, and scfv16 were mixed in a molar ratio of 1:1.2:1.2:1.2 and incubated for 1 h at room temperature for the formation of 5-HT$_6$R-Gs complex. The sample was purified over a Superdex 200 10/300 GL column and concentrated using a 100 kDa concentrator (details are provided in *SI Appendix, Materials and Methods*).

Cryo-EM Sample Preparation, Data Acquisition, and Structure Determination. The 5-HT$_6$R-Gs complex sample was applied onto a plasma-cleaned holey carbon grid (Quantifoil R1.2/1.3 Au, 200 mesh) at the concentration of 7.5 mg/mL and the cryo-EM movies were collected on a Titan Krios electron microscope (Thermo Fisher Scientific) operated at an accelerating voltage of 300 kV with a magnification of 64,000×. The data processing was performed in RELION 3.1 and obtained a final map at 3.0-Å resolution (details are provided in *SI Appendix, Materials and Methods* and Fig. S2)

Bioluminescence Resonance Energy Transfer Assay (BRET). HEK293T cells were trancfected with a 1:4 ratio of receptor-Rluc8:GFP2-mini-Gs for 5-HT$_6$R-mediated Gs protein activation, a 1:5 ratio of receptor-Rluc8:GFP2-β-arrestin2 for 5-HT$_6$R-mediated β-arrestin2 recruitment and a 1:10 ratio of receptor-Rluc8:GFP2-nanobody for nanobody screening. After 24 h, cells were plated in white opaque bottom 96-well assay plates and the next day incubated with 7.5 μM coelenterazine 400a and compounds for 5 min followed by read in an LB940 Mithras plate reader (Berthold Technologies) with 395-nm and 510-nm emission filters (details are provided in *SI Appendix, Materials and Methods*).

β-Arrestin2 Recruitment Tango Assays. To measure 5-HT$_6$R mediated β-arrestin2 translocation activity, Tango assay was used as previously described (41). 5-HT$_6$R Tango construct was fused the TEV cleavage site and the tetracycline transactivator (tTA) to the C terminus of the receptor. HTLA cells, expressing TEV fused β-arrestin2 and a tetracycline transactivator-driven luciferase, were maintained in dulbecco's modified eagle medium (DMEM), supplemented with 10% fetal bovine serum (FBS), 5 mg/mL Puromycin and 100 mg/mL Hygromycin B. HTLA cells were transfected with 5-HT$_6$R Tango construct and the next day were plated in 384-well white clear bottom cell culture plates at a density of 10,000 cells/well in a volume of 30 μL per well in DMEM containing 2% dialyzed FBS. Drug stimulation solutions were prepared in drug buffer at 4× concentration and added to cells (10 μL per well) for at least 18 h incubation. On the day of measurement, the medium was removed and 20 μL per well of BrightGlo reagent (Promega, diluted 20-fold with drug buffer) was added. The plates were incubated for 20 min at room temperature in the dark and then counted on Envision luminescence counter (PerkinElmer).

cAMP Assays. To measure 5-HT$_6$R mediated cAMP production, GloSensor cAMP Assay (Promega) was used. 5-HT$_6$R expression construct cloned into pcDNA3.1 vector and the GloSensor cAMP DNA construct were cotransfected into HEK293T cells in six-well dishes overnight. The cells were seeded into white opaque bottom 96-well assay plates in DMEM supplemented with 2% dialyzed FBS at a density of 30,000 to 50,000 cells /well in a volume of 100 μL per well. After at least 18 h, cells were removed from culture medium and loaded with 40 μL drug buffer at room temperature for 10 min. The plates were added 20 μL of 4 mM luciferin prepared in drug buffer following 20 μL of 3× drug solutions were incubated for 10 min. The chemiluminescence was counted after 5 min on Envision luminescence counter (PerkinElmer).

Radioligand-Binding Assay. For displacement experiments, HEK293T membranes expressing the human 5-HT$_6$R or the different mutants were prepared and incubated with [^{3}H]-LSD (0.8 to 1.0 nM) and increasing concentrations of compounds for 1.5 h at room temperature in the dark. The reaction was terminated by rapid vacuum filtration onto chilled 0.3% PEI-soaked GF/A filters. Counts per minute (CPM) was counted on MicroBeta TriLux reader (PerkinElmer). Saturation binding assays with 0.2 to 20 nM [^{3}H]-LSD in 5-HT$_6$R standard-binding buffer were performed to determine equilibrium dissociation constants (K_d), whereas 10 μM lisuride was used to define nonspecific binding. The reaction was incubated in dark for 1.5 h and terminated by rapid vacuum filtration. To examine the effects of sodium on ligand binding at 5-HT$_6$R, the assays were conducted in binding buffer (20 mM HEPES, 1 mM $MgCl_2$, 1 mM EDTA) in the absence or presence of

50 mM, 150 mM, or 300 mM NaCl and the members were incubated with 20 nM [^{3}H]-LSD. 10 μM lisuride was used to define nonspecific binding. (Details are provided in *SI Appendix, Materials and Methods*.)

Receptor Surface Expression Detection. The receptor surface expression level was detected by the nanoluc system according to Nano-Glo® HiBiT Extracellular Detection System (Promega). HEK293T cells were transfected with 1 μg/well N-terminal HiBiT-tagged receptor construct in 12-well plates. After 18 to 24 h, cells were plated into 384-well white clear-bottom plates in DMEM containing 2% dialyzed FBS (12,000 cells in 30 μL/well, quadruplicate each receptor) and incubated overnight. On the day of measurement, medium was removed and 20 μL assay buffer (containing 20 nM LgBiT protein and 10 μM furimazine substrate) was added to each well and incubated for 10 min before count on Ensight luminescence counter (PerkinElmer). The expression level was presented as percentage relative to the wild-type receptor.

Data, Materials, and Software Availability. All study data are included in the article and *SI Appendix*. The Cryo-EM map and corresponding atomic coordinates model for the serotonin-bound 5-HT$_6$R-Gs complex structure has been deposited in the Electron Microscopy Data Bank with accession codes of EMD-34073 (42) and RCSB Protein Data Bank with identification code of 7YS6 (43), respectively.

ACKNOWLEDGMENTS. This work was supported by the National Key R&D Programs of China (2020YFA0509600 and 2017YFA0503503), the National Natural Science Foundation of China (82225025, 32071197, 31872714, 31861143028, and 32130056), the CAS Strategic Priority Research Program (XDB19020111 and XDB37040103) to S.W. and Y.C.; The Shanghai Rising-Star Program (20QA1410600) and Thousand Talents Plan-Youth to S.W.; Shanghai Academic Research Leader (20XD1404200) and the CAS Facility-based Open Research Program to Y.C. The cryo-EM data were collected at the National Center for Protein Science Shanghai (NCPSS). We are grateful to the staffs of the NCPSS Electron Microscopy facility, Data base and Computing facility for instrument support and technical assistance.

Author affiliations: [a]State Key Laboratory of Molecular Biology, Shanghai Institute of Biochemistry and Cell Biology, Center for Excellence in Molecular Cell Science, Chinese Academy of Sciences, University of Chinese Academy of Sciences, Shanghai 200031, China

1. D. Hoyer, J. P. Hannon, G. R. Martin, Molecular, pharmacological and functional diversity of 5-HT receptors. *Pharmacol. Biochem. Behav.* **71**, 533–554 (2002).
2. M. Berger, J. A. Gray, B. L. Roth, The expanded biology of serotonin. *Annu. Rev. Med.* **60**, 355–366 (2009).
3. S. Fidalgo, D. K. Ivanov, S. H. Wood, Serotonin: From top to bottom. *Biogerontology* **14**, 21–45 (2013).
4. F. J. Monsma Jr., Y. Shen, R. P. Ward, M. W. Hamblin, D. R. Sibley, Cloning and expression of a novel serotonin receptor with high affinity for tricyclic psychotropic drugs. *Mol. Pharmacol.* **43**, 320–327 (1993).
5. M. Ruat *et al.*, A novel rat serotonin (5-HT6) receptor: Molecular cloning, localization and stimulation of cAMP accumulation. *Biochem. Biophys. Res. Commun.* **193**, 268–276 (1993).
6. B. Benhamu, M. Martin-Fontecha, H. Vazquez-Villa, L. Pardo, M. L. Lopez-Rodriguez, Serotonin 5-HT6 receptor antagonists for the treatment of cognitive deficiency in alzheimer's disease. *J. Med. Chem.* **57**, 7160–7181 (2014).
7. D. Marazziti *et al.*, Serotonin receptors of type 6 (5-HT6): From neuroscience to clinical pharmacology. *Curr. Med. Chem.* **20**, 371–377 (2013).
8. I. E. M. de Jong, A. Mork, Antagonism of the 5-HT6 receptor–preclinical rationale for the treatment of alzheimer's disease. *Neuropharmacology* **125**, 50–63 (2017).
9. R. Khoury, N. Grysman, J. Gold, K. Patel, G. T. Grossberg, The role of 5 HT6-receptor antagonists in alzheimer's disease: An update. *Expert Opin. Investig. Drugs* **27**, 523–533 (2018).
10. N. M. de Bruin, C. G. Kruse, 5-HT6 receptor antagonists: Potential efficacy for the treatment of cognitive impairment in schizophrenia. *Curr. Pharm. Des.* **21**, 3739–3759 (2015).
11. R. Kohen, L. A. Fashingbauer, D. E. Heidmann, C. R. Guthrie, M. W. Hamblin, Cloning of the mouse 5-HT6 serotonin receptor and mutagenesis studies of the third cytoplasmic loop. *Brain Res. Mol. Brain. Res.* **90**, 110–117 (2001).
12. M. Teitler, K. Herrick-Davis, A. Purohit, Constitutive activity of G-protein coupled receptors: Emphasis on serotonin receptors. *Curr. Top. Med. Chem.* **2**, 529–538 (2002).
13. W. Deraredj Nadim *et al.*, Physical interaction between neurofibromin and serotonin 5-HT6 receptor promotes receptor constitutive activity. *Proc. Natl. Acad. Sci. U.S.A.* **113**, 12310–12315 (2016).
14. F. Duhr *et al.*, Cdk5 induces constitutive activation of 5-HT6 receptors to promote neurite growth. *Nat. Chem. Biol.* **10**, 590–597 (2014).
15. M. Jacobshagen, M. Niquille, S. Chaumont-Dubel, P. Marin, A. Dayer, The serotonin 6 receptor controls neuronal migration during corticogenesis via a ligand-independent Cdk5-dependent mechanism. *Development* **141**, 3370–3377 (2014).
16. Q. Wang *et al.*, Constitutive activity of serotonin receptor 6 regulates human cerebral organoids formation and depression-like behaviors. *Stem Cell Rep.* **16**, 75–88 (2021).
17. P. Leff, The two-state model of receptor activation. *Trends Pharmacol. Sci.* **16**, 89–97 (1995).
18. S. Maeda *et al.*, Development of an antibody fragment that stabilizes GPCR/G-protein complexes. *Nat. Commun.* **9**, 3712 (2018).
19. S. Maeda, Q. H. Qu, M. J. Robertson, G. Skiniotis, B. K. Kobilka, Structures of the M1 and M2 muscarinic acetylcholine receptor/G-protein complexes. *Science* **364**, 552 (2019).
20. K. Kim *et al.*, Structure of a hallucinogen-activated Gq-coupled 5-HT2A serotonin receptor. *Cell* **182**, 1574 (2020).
21. S. G. Rasmussen *et al.*, Crystal structure of the beta2 adrenergic receptor-Gs protein complex. *Nature* **477**, 549–555 (2011).
22. W. I. Weis, B. K. Kobilka, The molecular basis of G protein-coupled receptor activation. *Annu. Rev. Biochem.* **87**, 897–919 (2018).
23. A. Koehl *et al.*, Structure of the micro-opioid receptor-Gi protein complex. *Nature* **558**, 547–552 (2018).
24. X. Y. Liu *et al.*, Mechanism of intracellular allosteric beta(2)AR antagonist revealed by X-ray crystal structure. *Nature* **548**, 480 (2017).
25. K. Kristiansen *et al.*, A highly conserved aspartic acid (Asp-155) anchors the terminal amine moiety of tryptamines and is involved in membrane targeting of the 5-HT2A serotonin receptor but does not participate in activation via a "salt-bridge disruption" mechanism. *J. Pharmacol. Exp. Therapeut.* **293**, 735–746 (2000).
26. V. Katritch, V. Cherezov, R. C. Stevens, Structure-function of the G protein-coupled receptor superfamily. *Annu. Rev. Pharmacol.* **53**, 531–556 (2013).
27. V. Katritch *et al.*, Allosteric sodium in class A GPCR signaling. *Trends Biochem. Sci.* **39**, 233–244 (2014).
28. Q. T. Zhou *et al.*, Common activation mechanism of class A GPCRs. *Elife* **8**, e50279 (2019).
29. B. Carpenter, R. Nehme, T. Warne, A. G. Leslie, C. G. Tate, Structure of the adenosine A(2A) receptor bound to an engineered G protein. *Nature* **536**, 104–107 (2016).
30. D. P. Staus *et al.*, Structure of the M2 muscarinic receptor-beta-arrestin complex in a lipid nanodisc. *Nature* **579**, 297–302 (2020).
31. Y. Lee *et al.*, Molecular basis of beta-arrestin coupling to formoterol-bound beta1-adrenoceptor. *Nature* **583**, 862–866 (2020).
32. P. Y. Xu *et al.*, Structural insights into the lipid and ligand regulation of serotonin receptors. *Nature* **592**, 469–473 (2021).
33. Y. W. Zhuang *et al.*, Mechanism of dopamine binding and allosteric modulation of the human D1 dopamine receptor. *Cell Res.* **31**, 593–596 (2021).
34. S. Wang *et al.*, Structure of the D2 dopamine receptor bound to the atypical antipsychotic drug risperidone. *Nature* **555**, 269–273 (2018).
35. V. Katritch *et al.*, Allosteric sodium in class A GPCR signaling. *Trends Biochem. Sci.* **39**, 233–244 (2014).
36. S. Wang *et al.*, D4 dopamine receptor high-resolution structures enable the discovery of selective agonists. *Science* **358**, 381–386 (2017).
37. T. Flock *et al.*, Universal allosteric mechanism for Galpha activation by GPCRs. *Nature* **524**, 173–179 (2015).
38. G. G. Gregorio *et al.*, Single-molecule analysis of ligand efficacy in beta2AR-G-protein activation. *Nature* **547**, 68–73 (2017).
39. X. Y. Liu *et al.*, Structural insights into the process of GPCR-G protein complex formation. *Cell* **177**, 1243 (2019).
40. E. Pardon *et al.*, A general protocol for the generation of nanobodies for structural biology. *Nat. Protoc.* **9**, 674–693 (2014).
41. W. K. Kroeze *et al.*, PRESTO-tango as an open-source resource for interrogation of the druggable human GPCRome. *Nat. Struct. Mol. Biol.* **22**, 362–369 (2015).
42. L. He *et al.*, Structural insights into constitutive activity of 5-HT6 receptor. *Electron Microscopy Data Bank*. https://www.emdataresource.org/EMD-34073. Deposited 11 August 2022.
43. L. He *et al.*, Structural insights into constitutive activity of 5-HT6 receptor. RCSB Protein Data Bank. https://www.rcsb.org/structure/unreleased/7YS6. Deposited 11 August 2022.